Appl. Math. Mech. -Engl. Ed., **36**(3), 337–352 (2015)
DOI 10.1007/s10483-015-1919-6
©Shanghai University and Springer-Verlag
Berlin Heidelberg 2015

Applied Mathematics and Mechanics (English Edition)

Integral treatment for forced convection heat and mass transfer of nanofluids over linear stretching sheet*

A. NOGHREHABADI†, P. SALAMAT, M. GHALAMBAZ

Department of Mechanical Engineering, Shahid Chamran
University of Ahvaz, Ahvaz 6135743337, Iran

Abstract An integral treatment is proposed for the analysis of the forced convection flow of a nanofluid over a stretching sheet. The obtained results agree well with the numerical results. The results of the presented solution provide an analytic solution, which can be conveniently used in engineering applications. Four types of nanoparticles, i.e., alumina (Al_2O_3), silicon dioxide (SiO_2), silver (Ag), and copper (Cu), dispersed in the base fluid of water are examined. The analytical results show that an increase in the volume fraction of nanoparticles increases the thickness of the thermal boundary layer. The reduced Nusselt number is a decreasing function of the volume fraction of nanoparticles.

Key words nanofluid, integral method, stretching sheet, analytical solution, thermal enhancement

Chinese Library Classification O353.4
2010 Mathematics Subject Classification 74F10, 76N20, 76A05

Nomenclature

$(\rho c)_{\rm f}$,	heat capacity of the fluid;
$(\rho c)_{\rm p}$,	effective heat capacity of the nanoparticle material;
$(\rho c_p)_{\rm nf}$,	heat capacity of the nanofluid;
∞,	condition at infinity;
$D_{\rm B}$,	Brownian diffusion coefficient;
$d_{\rm p}$,	nanoparticle diameter;
$D_{\rm T}$,	thermophoretic diffusion coefficient;
g,	gravitational acceleration vector;
h,	local heat transfer coefficient;
$h_{\rm m}$,	local mass transfer coefficient;
$h_{\rm nf}$,	heat transfer coefficient of the nanofluid;
K,	thermal conductivity;
$K_{\rm B}$,	Boltzmann constant;
$k_{\rm f}$,	thermal conductivity of the fluid;
$k_{\rm nf}$,	nanofluid thermal conductivity;
$k_{\rm p}$,	nanoparticle thermal conductivity;
Le,	Lewis number;
$N_{\rm B}$,	Brownian motion parameter;
$N_{\rm T}$,	thermophoresis parameter;
Nu,	Nusselt number;
P,	pressure;
Pr,	Prandtl number;
Re_x,	local Reynolds number;
Sh_x,	local Sherwood number;
T,	temperature;
T_∞,	ambient temperature attained as y tends to infinity;
$T_{\rm w}$,	temperature at the stretching surface;
u, v,	velocity components;
$u_{\rm w}$,	velocity of the stretching sheet;
w,	condition at the stretching surface;

* Received May 15, 2014 / Revised Aug. 1, 2014
† Corresponding author, E-mail: noghrehabadi@scu.ac.ir

x, y,	Cartesian coordinates;	$\mu_{\rm nf}$,	viscosity of the nanofluid;
α,	thermal diffusivity;	$\rho_{\rm f}$,	fluid density;
β,	volumetric expansion coefficient of the fluid;	$\rho_{\rm nf}$,	nanofluid density;
		$\rho_{\rm p}$,	nanoparticle mass density;
Δ,	boundary-layer thickness ratio;	υ,	kinematic viscosity of the fluid;
δ_c,	concentration boundary-layer thickness;	φ,	nanoparticle volume fraction;
$\delta_{\rm T}$,	thermal boundary-layer thickness;	$\varphi(\eta)$,	dimensionless concentration profile;
τ,	heat capacity ration $(\rho c)_{\rm p}/(\rho c)_{\rm f}$;	φ_∞,	ambient concentration attained as y tends to infinity;
$\theta(\eta)$,	dimensionless temperature profile;		
$\mu_{\rm f}$,	viscosity of the fluid;	$\varphi_{\rm w}$,	ambient nanoparticle volume fraction.

1 Introduction

The analysis of the boundary layer flow and convective heat transfer passing a stretching surface is very important in many industrial processes. The stretching phenomena occur in a number of manufacturing processes in modern industry, e.g., metal and polymer extrusion, hot rolling, drawing of plastic sheets, paper production, and continuous casting[1–2]. In many metallurgical processes such as drawing of continuous filaments through quiescent fluids and annealing and tinning of copper wires, the properties of the final product depend greatly on the rate of cooling or heating involved in these processes[3]. Therefore, the rate of heat transfer from the sheet and consequently the choice of a proper working liquid can significantly affect the quality of the final product.

Recently, the study of the boundary layer flow and convective heat transfer in nanofluids has gained a lot of attention because of the unique thermal properties of these fluids. Nanofluids were first introduced in 1995 by Choi[4]. They are solid-liquid composite materials consisting of solid nanoparticles or nanofibers with sizes typically in the range from 1 nm to 100 nm, suspending in a liquid. The dramatically enhancement of the thermal conductivity of nanofluids, which can be achieved by dispersing a low volume fraction of host nanoparticles, has attracted the attention of many researchers. A small amount (<1% volume fraction) of Cu nanoparticles or carbon nanotubes, dispersed in ethylene glycol or oil, can increase the inherently poor thermal conductivity of the liquid by 40% and 150%, respectively[5–6]. Conventional particle liquid suspensions require high particle concentration (>10%) in the size of millimeter or micrometer so as to achieve such enhancement. Nanofluids have many applications in industries since materials of nanometer size have unique physical and thermal properties. Sun et al.[7] introduced a new correlation based on their measured data to predict the effective thermal conductivity of the nanofluids, considering the effects of the flow shear rate, the nanoparticle diameter, and the nanoparticle volume fraction.

Sakiadis[8] analyzed the boundary layer flow over a continuous surface. Crane[9] obtained an exact solution for the boundary layer flow of a Newtonian fluid caused by the stretching of an elastic sheet moving in its own plane linearly. Tsou et al.[10] extended the research to the heat transfer phenomenon of the boundary layer flow over a continuous moving surface. Magyari and Keller[11–12] studied the thermal boundary layer of moving surfaces. Wang[13] studied the free convection from a vertical stretching surface. Gorla and Sidawi[14] analyzed the characteristics of flow and heat transfer from a continuous surface with suction and blowing.

Very recently, different aspects of the flow and heat transfer of nanofluids over a stretching sheet have been analyzed numerically. Khan and Pop[15] studied the laminar boundary layer flow and heat transfer of nanofluids over a linear stretching sheet. Makinde and Aziz[16] assumed that the sheet was thin and subject to a convective flow from below. Rana and Bhargava[17] assumed a non-linear velocity for the sheet. Noghrehabadi et al.[18] considered a slip velocity on the surface because of the presence of nanoparticles in the base fluid. Noghrehabadi

et al. examined the effect of magnetic field[19], heat generation[20], and convective boundary condition[21] on the boundary layer heat transfer of nanofluids over a linear stretching sheet. In all of the mentioned studies[15–21], the boundary layer approximations were utilized. The governing partial differential equations were first reduced to a set of highly non-linear ordinary differential equations, and then solved numerically.

Although the numerical methods are capable to obtain a reasonable solution for the boundary layer heat and mass transfer of nanofluids, they need a large amount of computation. Moreover, for each set of the non-dimensional parameters, the computation is repeated. In contrast with the numerical solutions, the analytic solutions can provide a closed form solution for the problem. In many engineering applications, a simple relation which clearly shows the relation between the main characteristics of the problem and different non-dimensional parameters are highly demanded. Using such a simple analytic relation, engineers can easily and rapidly calculate the physical characteristics of heat and mass transfer for any arbitrary value of non-dimensional parameters.

In the present study, an integral method is utilized to analyze the boundary layer flow and heat transfer of nanofluids along an isothermal stretching sheet. An integral solution, depending on four dimensionless parameters, i.e., the Lewis number, the Prandtl number, the Brownian motion parameter, and the thermophoresis parameter, is obtained and analytically solved. The effect of different types of nanoparticles, namely, silicon dioxide (SiO_2), silver (Ag), alumina (Al_2O_3), and copper (Cu), on the thermal enhancement of water based nanofluids over an isothermal stretching sheet is studied.

2 Problem definition and mathematical formulation

Consider the steady-state force convection boundary-layer flow of a water base nanofluid along an isothermal stretching sheet. The nanofluid can contain different volume fractions of nanoparticles. The x-coordinate is measured from the leading edge of the sheet, and the y-coordinate is measured normal to the sheet. Figure 1 shows a schematic view of the stretching sheet and the coordinate system. The surface of the stretching sheet is maintained at a constant temperature of T_w. The volume fraction of nanoparticles at the surface φ_w is assumed to be constant. The nanoparticle volume fraction and the temperature of the nanofluid far from the surface (ambient) are denoted by φ_∞ and T_∞, respectively.

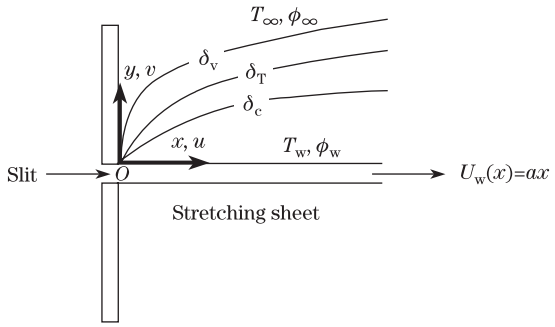

Fig. 1 Physical model and coordinate system

It is assumed that: (a) the flow is steady and incompressible, (b) the boundary layer approximations are applicable, and (c) the nanoparticles and the base fluid are in local thermal equilibrium. With these assumptions, the governing boundary layer equations of mass, momen-

tum, energy, and concentration of the nanoparticles can be written as follows[15]:

$$\frac{\partial u}{\partial x}+\frac{\partial v}{\partial y}=0, \tag{1}$$

$$u\frac{\partial u}{\partial x}+v\frac{\partial u}{\partial y}=-\frac{1}{\rho_{\mathrm{f}}}\frac{\partial p}{\partial x}+\nu\Big(\frac{\partial^2 u}{\partial x^2}+\frac{\partial^2 u}{\partial y^2}\Big), \tag{2}$$

$$u\frac{\partial v}{\partial x}+v\frac{\partial v}{\partial y}=-\frac{1}{\rho_{\mathrm{f}}}\frac{\partial p}{\partial y}+\nu\Big(\frac{\partial^2 v}{\partial x^2}+\frac{\partial^2 v}{\partial y^2}\Big), \tag{3}$$

$$\begin{aligned}&u\frac{\partial T}{\partial x}+v\frac{\partial T}{\partial y}\\&=\frac{(\rho c)_{\mathrm{p}}}{(\rho c)_{\mathrm{f}}}\Big(D_{\mathrm{B}}\Big(\frac{\partial\varphi}{\partial x}\frac{\partial T}{\partial x}+\frac{\partial\varphi}{\partial y}\frac{\partial T}{\partial y}\Big)+\frac{D_{\mathrm{T}}}{T_\infty}\Big(\Big(\frac{\partial T}{\partial x}\Big)^2+\Big(\frac{\partial T}{\partial y}\Big)^2\Big)\Big)\\&\quad+\alpha\Big(\frac{\partial^2 T}{\partial x^2}+\frac{\partial^2 T}{\partial y^2}\Big),\end{aligned} \tag{4}$$

$$u\frac{\partial\varphi}{\partial x}+v\frac{\partial\varphi}{\partial y}=D_{\mathrm{B}}\Big(\frac{\partial^2\varphi}{\partial x^2}+\frac{\partial^2\varphi}{\partial y^2}\Big)+\frac{D_{\mathrm{T}}}{T_\infty}\Big(\frac{\partial^2 T}{\partial x^2}+\frac{\partial^2 T}{\partial y^2}\Big), \tag{5}$$

where u and v are the volume-averaged velocity components in the x- and y-directions, respectively. T and φ denote the temperature and the volume fraction of nanoparticles, respectively. ρ_{f} is the density of the base fluid, α is the thermal diffusivity, and ν is the kinematic viscosity. ρ_{p} is the density of the particles. $(\rho c)_{\mathrm{f}}$ is the heat capacity of the nanofluid, and $(\rho c)_{\mathrm{p}}$ is the effective heat capacity of the nanoparticles. D_{B} and D_{T} are the Brownian diffusion coefficient and the thermophoresis diffusion coefficient, respectively. The boundary conditions are

$$v=0,\quad u=u_{\mathrm{w}}(x)=ax,\quad T=T_{\mathrm{w}},\quad \varphi=\varphi_{\mathrm{w}}\quad\text{at}\quad y=0, \tag{6}$$

$$u=v=0,\quad T=T_\infty,\quad \varphi=\varphi_\infty\quad\text{at}\quad y\to\infty. \tag{7}$$

To attain an integral solution, the energy equation (4) and the conservation equation (5) can be rewritten as follows:

$$\frac{\partial(uT)}{\partial x}+\frac{\partial(vT)}{\partial y}-T\Big(\frac{\partial v}{\partial y}+\frac{\partial u}{\partial x}\Big)=\alpha\frac{\partial^2 T}{\partial y^2}+\tau\Big(D_{\mathrm{B}}\frac{\partial\varphi}{\partial y}\frac{\partial T}{\partial y}+\frac{D_{\mathrm{T}}}{T_\infty}\Big(\frac{\partial T}{\partial y}\Big)^2\Big), \tag{8}$$

$$\frac{\partial(u\varphi)}{\partial x}-\varphi\Big(\frac{\partial u}{\partial x}+\frac{\partial v}{\partial x}\Big)+\frac{\partial(v\varphi)}{\partial x}=D_{\mathrm{B}}\frac{\partial^2\varphi}{\partial y^2}+\frac{D_{\mathrm{T}}}{T_\infty}\frac{\partial^2 T}{\partial y^2}, \tag{9}$$

where

$$\tau=\frac{(\rho c)_{\mathrm{p}}}{(\rho c)_{\mathrm{f}}}.$$

Now, with the continuity equation, Eqs. (1), (8), and (9) can be reduced to

$$\frac{\partial(uT)}{\partial x}+\frac{\partial(vT)}{\partial y}=\alpha\frac{\partial^2 T}{\partial y^2}+\tau D_{\mathrm{B}}\frac{\partial\varphi}{\partial y}\frac{\partial T}{\partial y}+\tau\frac{D_{\mathrm{T}}}{T_\infty}\Big(\frac{\partial T}{\partial y}\Big)^2, \tag{10}$$

$$\frac{\partial(u\varphi)}{\partial x}+\frac{\partial(v\varphi)}{\partial x}=D_{\mathrm{B}}\frac{\partial^2\varphi}{\partial y^2}+\frac{D_{\mathrm{T}}}{T_\infty}\frac{\partial^2 T}{\partial y^2}. \tag{11}$$

Integrating the above equations and using the Leibniz integral rule yield

$$\begin{aligned}&\frac{\mathrm{d}}{\mathrm{d}x}\int_0^\infty uT\mathrm{d}y+\int_0^\infty\frac{\partial}{\partial y}(\upsilon T)\mathrm{d}y\\&=\alpha\int_0^\infty\frac{\partial^2T}{\partial y^2}\mathrm{d}y+\tau D_\mathrm{B}\int_0^\infty\frac{\partial\varphi}{\partial y}\frac{\partial T}{\partial y}\mathrm{d}y+\tau\frac{D_\mathrm{T}}{T_\infty}\int_0^\infty\Big(\frac{\partial T}{\partial y}\Big)^2\mathrm{d}y,\end{aligned}\tag{12}$$

$$\begin{aligned}&\frac{\mathrm{d}}{\mathrm{d}x}\int_0^\infty u\varphi\,\mathrm{d}y+\int_0^\infty\frac{\partial}{\partial y}(\upsilon\varphi)\mathrm{d}y\\&=D_\mathrm{B}\int_0^\infty\frac{\partial^2\varphi}{\partial y^2}\mathrm{d}y+\frac{D_\mathrm{T}}{T_\infty}\int_0^\infty\frac{\partial^2T}{\partial y^2}\mathrm{d}y.\end{aligned}\tag{13}$$

They can be further simplified as follows:

$$\begin{aligned}&\frac{\mathrm{d}}{\mathrm{d}x}\int_0^\infty uT\mathrm{d}y+T_\infty\upsilon_\infty-T_0\upsilon_0\\&=\alpha\Big(\frac{\partial T}{\partial y}\Big)_\infty-\alpha\Big(\frac{\partial T}{\partial y}\Big)_0+\tau D_\mathrm{B}\int_0^\infty\frac{\partial\varphi}{\partial y}\frac{\partial T}{\partial y}\mathrm{d}y+\tau\frac{D_\mathrm{T}}{T_\infty}\int_0^\infty\Big(\frac{\partial T}{\partial y}\Big)^2\mathrm{d}y,\end{aligned}\tag{14}$$

$$\begin{aligned}&\frac{\mathrm{d}}{\mathrm{d}x}\int_0^\infty(u\varphi)\mathrm{d}y+\upsilon_\infty\varphi_\infty-\upsilon_0\varphi_0\\&=D_\mathrm{B}\Big(\frac{\partial\varphi}{\partial y}\Big)_\infty-D_\mathrm{B}\Big(\frac{\partial\varphi}{\partial y}\Big)_0+\frac{D_\mathrm{T}}{T_\infty}\Big(\frac{\partial T}{\partial y}\Big)_\infty-\frac{D_\mathrm{T}}{T_\infty}\Big(\frac{\partial T}{\partial y}\Big)_0.\end{aligned}\tag{15}$$

Since the surface of the plate is impermeable and the flow outside the boundary layer is quiescent, it is assumed that

$$\Big(\frac{\partial(\cdot)}{\partial y}\Big)_\infty=0,\quad\upsilon_0=0.$$

With these assumptions, Eqs. (14) and (15) can be simplified as follows:

$$\begin{aligned}&\frac{\mathrm{d}}{\mathrm{d}x}\int_0^\infty uT\mathrm{d}y+T_\infty\upsilon_\infty\\&=-\alpha\Big(\frac{\partial T}{\partial y}\Big)_0+\tau D_\mathrm{B}\int_0^\infty\frac{\partial\varphi}{\partial y}\frac{\partial T}{\partial y}\mathrm{d}y+\tau\frac{D_\mathrm{T}}{T_\infty}\int_0^\infty\Big(\frac{\partial T}{\partial y}\Big)^2\mathrm{d}y,\end{aligned}\tag{16}$$

$$\frac{\mathrm{d}}{\mathrm{d}x}\int_0^\infty(u\varphi)\mathrm{d}y+\upsilon_\infty\varphi_\infty=-D_\mathrm{B}\Big(\frac{\partial\varphi}{\partial y}\Big)_0-\frac{D_\mathrm{T}}{T_\infty}\Big(\frac{\partial T}{\partial y}\Big)_0.\tag{17}$$

Similarly, integrating the continuity equation (1) from the surface to the outside of the boundary layer yields

$$\frac{\partial u}{\partial x}+\frac{\partial\upsilon}{\partial y}=0\ \Rightarrow\frac{\mathrm{d}}{\mathrm{d}x}\int_0^\infty u\mathrm{d}y+\upsilon_\infty-\upsilon_0=0\Rightarrow\upsilon_\infty=-\frac{\mathrm{d}}{\mathrm{d}x}\int_0^\infty u\mathrm{d}y.\tag{18}$$

Substituting v_∞ from Eq. (18) into Eqs. (16) and (17) yields

$$\begin{aligned}&\frac{\mathrm{d}}{\mathrm{d}x}\int_0^\infty uT\mathrm{d}y - T_\infty\frac{\mathrm{d}}{\mathrm{d}x}\int_0^\infty u\mathrm{d}y\\ =\ &-\alpha\Big(\frac{\partial T}{\partial y}\Big)_0 + \tau D_\mathrm{B}\int_0^\infty \frac{\partial\varphi}{\partial y}\frac{\partial T}{\partial y}\mathrm{d}y + \tau\frac{D_\mathrm{T}}{T_\infty}\int_0^\infty\Big(\frac{\partial T}{\partial y}\Big)^2\mathrm{d}y,\end{aligned}\tag{19}$$

$$\begin{aligned}&\frac{\mathrm{d}}{\mathrm{d}x}\int_0^\infty (u\varphi)\mathrm{d}y - \varphi_\infty\frac{\mathrm{d}}{\mathrm{d}x}\int_0^\infty u\,\mathrm{d}y\\ =\ &-D_\mathrm{B}\Big(\frac{\partial\varphi}{\partial y}\Big)_0 - \frac{D_\mathrm{T}}{T_\infty}\Big(\frac{\partial T}{\partial y}\Big)_0.\end{aligned}\tag{20}$$

The second terms on the left-hand side of Eqs. (19) and (20) can be derived as follows:

$$T_\infty\frac{\mathrm{d}}{\mathrm{d}x}\int_0^\infty u\mathrm{d}y = \frac{\mathrm{d}}{\mathrm{d}x}\int_0^\infty uT_\infty\mathrm{d}y - \frac{\mathrm{d}T_\infty}{\mathrm{d}x}\int_0^\infty u\mathrm{d}y,\tag{21}$$

$$\varphi_\infty\frac{\mathrm{d}}{\mathrm{d}x}\int_0^\infty u\mathrm{d}y = \frac{\mathrm{d}}{\mathrm{d}x}\int_0^\infty u\varphi_\infty\mathrm{d}y - \frac{\mathrm{d}\varphi_\infty}{\mathrm{d}x}\int_0^\infty u\mathrm{d}y.\tag{22}$$

Substituting the above equations into Eqs. (19) and (20) and considering that T_∞ and φ_∞ are constant yield

$$\begin{aligned}&\frac{\mathrm{d}}{\mathrm{d}x}\int_0^\infty u(T-T_\infty)\mathrm{d}y\\ =\ &-\alpha\Big(\frac{\partial T}{\partial y}\Big)_0 + \tau D_\mathrm{B}\int_0^\infty \frac{\partial\varphi}{\partial y}\frac{\partial T}{\partial y}\mathrm{d}y + \tau\frac{D_\mathrm{T}}{T_\infty}\int_0^\infty\Big(\frac{\partial T}{\partial y}\Big)^2\mathrm{d}y,\end{aligned}\tag{23}$$

$$\begin{aligned}&\frac{\mathrm{d}}{\mathrm{d}x}\int_0^\infty u(\varphi-\varphi_\infty)\,\mathrm{d}y\\ =\ &-D_\mathrm{B}\Big(\frac{\partial\varphi}{\partial y}\Big)_0 - \frac{D_\mathrm{T}}{T_\infty}\Big(\frac{\partial T}{\partial y}\Big)_0.\end{aligned}\tag{24}$$

The exact solution for the momentum equations (2) and (3), satisfying the boundary conditions (6) and (7), can be obtained as follows[8]:

$$u = ax\mathrm{e}^{-\sqrt{\frac{a}{\nu}}y},\tag{25}$$

$$v = -(a\nu)^{\frac{1}{2}}\big(1-\mathrm{e}^{-\sqrt{\frac{a}{\nu}}y}\big).\tag{26}$$

There is an exact solution for the velocity profile. Therefore, the profiles of the dimensionless temperature and concentration, satisfying the boundary conditions (6) and (7), are assumed as follows:

$$\frac{T-T_\infty}{T_\mathrm{w}-T_\infty} = \mathrm{erfc}\Big(\frac{y}{\delta_\mathrm{T}}\Big),\tag{27}$$

$$\frac{\varphi-\varphi_\infty}{\varphi_\mathrm{w}-\varphi_\infty} = \mathrm{erfc}\Big(\frac{\Delta y}{\delta_\mathrm{T}}\Big),\tag{28}$$

where δ_T is the thermal boundary layer thickness, Δ is the ratio of the thermal boundary layer thickness to the concentration boundary layer thickness δ_c, and erfc is the complementary error function.

Substituting Eqs. (25), (26), (27), and (28) into Eqs. (23) and (24) yields

$$\begin{aligned}
&\frac{\mathrm{d}}{\mathrm{d}x}\int_0^\infty ax\mathrm{e}^{-\beta y}(T_\mathrm{w}-T_\infty)\mathrm{erfc}\Big(\frac{y}{\delta_\mathrm{T}}\Big)\mathrm{d}y\\
=&-\alpha(T_\mathrm{w}-T_\infty)\frac{\partial(\mathrm{erfc}(\frac{y}{\delta_\mathrm{T}}))}{\partial y}\Big|_{y=0}+\tau D_\mathrm{B}(T_\mathrm{w}-T_\infty)(\varphi_\mathrm{w}-\varphi_\infty)\\
&\cdot\int_0^\infty\frac{\partial(\mathrm{erfc}(\frac{y}{\delta_\mathrm{T}}))}{\partial y}\frac{\partial(\mathrm{erfc}(\frac{\Delta y}{\delta_\mathrm{T}}))}{\partial y}\mathrm{d}y\\
&+\tau\frac{D_\mathrm{T}}{T_\infty}(T_\mathrm{w}-T_\infty)^2\int_0^\infty\Big(\frac{\partial(\mathrm{erfc}(\frac{y}{\delta_\mathrm{T}}))}{\partial y}\Big)^2\mathrm{d}y, \qquad (29)\\
&\frac{\mathrm{d}}{\mathrm{d}x}\int_0^\infty ax\mathrm{e}^{-\beta y}(\varphi_\mathrm{w}-\varphi_\infty)\mathrm{erfc}\Big(\frac{\Delta y}{\delta_\mathrm{T}}\Big)\mathrm{d}y\\
=&-D_\mathrm{B}(\varphi_\mathrm{w}-\varphi_\infty)\frac{\partial(\mathrm{erfc}(\frac{\Delta y}{\delta_\mathrm{T}}))}{\partial y}\Big|_{y=0}\\
&-\frac{D_\mathrm{T}}{T_\infty}(T_\mathrm{w}-T_\infty)\frac{\partial(\mathrm{erfc}(\frac{y}{\delta_\mathrm{T}}))}{\partial y}\Big|_{y=0}. \qquad (30)
\end{aligned}$$

After simplifying Eqs. (29) and (30), the following two ordinary differential equations can be obtained:

$$\begin{aligned}
&\frac{\mathrm{d}}{\mathrm{d}x}\Big(\frac{ax}{\beta}\Big(\mathrm{e}^{\frac{\delta_\mathrm{T}^2\beta^2}{4}}\Big(-1+\mathrm{erfc}\Big(\frac{1}{2}\delta_\mathrm{T}\beta\Big)\Big)+1\Big)\Big)\\
=&\tau D_\mathrm{B}(\varphi_\mathrm{w}-\varphi_\infty)\frac{2}{\sqrt{\pi}}\frac{\Delta}{\sqrt{\Delta^2+1}}\frac{1}{\delta_\mathrm{T}}\\
&+\tau\frac{D_\mathrm{T}}{T_\infty}(T_\mathrm{w}-T_\infty)\sqrt{\frac{2}{\pi}}\frac{1}{\delta_\mathrm{T}}+\frac{2\alpha}{\sqrt{\pi}\delta_\mathrm{T}}, \qquad (31)\\
&\frac{\mathrm{d}}{\mathrm{d}x}\Big(\frac{ax}{\beta}\Big(\mathrm{e}^{\frac{\delta_\mathrm{T}^2\beta^2}{4\Delta^2}}\mathrm{erfc}\Big(\frac{\delta_\mathrm{T}\beta}{2\Delta}\Big)+1\Big)\Big)\\
=&D_\mathrm{B}\frac{2\Delta}{\sqrt{\pi}\delta_\mathrm{T}}+\frac{D_\mathrm{T}}{T_\infty}\frac{T_\mathrm{w}-T_\infty}{\varphi_\mathrm{w}-\varphi_\infty}\frac{2}{\sqrt{\pi}\delta_\mathrm{T}}. \qquad (32)
\end{aligned}$$

Based on the scale analysis, the thermal boundary layer thickness can be written as follows[22]:

$$\delta_\mathrm{T}=\frac{x}{Re_x^{\frac{1}{2}}}\delta_\mathrm{T}^*, \qquad (33)$$

where δ_T^* is a constant, and

$$Re_x=\frac{x}{\upsilon}u_\mathrm{w}(x).$$

Substituting the above expression for δ_{T} in Eqs. (31) and (32) yields

$$\delta_{\mathrm{T}}^{*}\mathrm{e}^{\frac{\delta_{\mathrm{T}}^{*2}}{4}}\left(-1+\operatorname{erfc}\left(\frac{1}{2}\delta_{\mathrm{T}}^{*}\right)\right)+\delta_{\mathrm{T}}^{*}$$

$$=\frac{2}{\sqrt{\pi}Pr}+\frac{2N_{\mathrm{B}}}{\sqrt{\pi}}\frac{\Delta}{\sqrt{\Delta^{2}+1}}+\sqrt{\frac{2}{\pi}}N_{\mathrm{T}}, \tag{34}$$

$$\delta_{\mathrm{T}}^{*}\mathrm{e}^{\frac{\delta_{\mathrm{T}}^{*2}}{4\Delta^{2}}}\left(-1+\operatorname{erfc}\left(\frac{1}{2\Delta}\delta_{\mathrm{T}}^{*}\right)\right)+\delta_{\mathrm{T}}^{*}$$

$$=\frac{2\Delta}{\sqrt{\pi}Le}+\frac{2}{\sqrt{\pi}}\frac{N_{\mathrm{T}}}{N_{\mathrm{B}}Le}, \tag{35}$$

where

$$N_{\mathrm{B}}=\frac{(\rho C)_{\mathrm{p}}D_{\mathrm{B}}(\varphi_{\mathrm{w}}-\varphi_{\infty})}{(\rho C)_{\mathrm{f}}\upsilon_{\mathrm{nf}}}, \tag{36}$$

$$N_{\mathrm{T}}=\frac{(\rho C)_{\mathrm{p}}D_{\mathrm{T}}(T_{\mathrm{w}}-T_{\infty})}{(\rho C)_{\mathrm{f}}T_{\infty}\upsilon_{\mathrm{nf}}}, \tag{37}$$

$$Pr=\frac{\upsilon}{\alpha}=\frac{c_{\mathrm{nf}}\mu_{\mathrm{nf}}}{k_{\mathrm{nf}}}, \tag{38}$$

$$Le=\frac{\upsilon_{\mathrm{nf}}}{D_{\mathrm{B}}}. \tag{39}$$

In the above equations, N_{B}, N_{T}, Pr, and Le represent the Brownian motion parameter, the thermophoresis parameter, the Prandtl number, and the Lewis number, respectively.

Now, Δ and δ_{T}^{*} can be obtained from the solution of Eqs. (34) and (35). The main parameters of interest are the reduced Nusselt number (Nu_{r}) and the reduced Sherwood number (Sh_{r}). The reduced Nusselt number, indicating the dimensionless rate of heat transfer from the surface, and the reduced Sherwood number, indicating the dimensionless rate of mass transfer from the surface, can be written as follows:

$$\begin{cases} Nu_{\mathrm{r}}=\dfrac{Nu_{x}}{Re_{x}^{\frac{1}{2}}}=\dfrac{1}{\delta_{\mathrm{T}}^{*}}, \\ Sh_{\mathrm{r}}=\dfrac{Sh_{x}}{Re_{x}^{\frac{1}{2}}}=\dfrac{\Delta}{\delta_{\mathrm{T}}^{*}}, \end{cases} \tag{40}$$

where

$$Nu_{x}=\frac{hx}{k},\quad Sh_{x}=\frac{h_{\mathrm{m}}x}{D_{\mathrm{B}}}.$$

In the above equations, h and h_{m} are the local heat transfer coefficient and the local mass transfer coefficient expressed by

$$h=\frac{k}{\delta_{\mathrm{T}}},\quad h_{\mathrm{m}}=\frac{D_{\mathrm{B}}}{\delta_{C}}.$$

The accuracy acquired in the above approximate expressions may be examined by comparing the heat and mass transfer results against the similarity solution. Our approximate formulae given by Eq. (40) tend to overestimate the heat and mass transfer rate under these physical

limiting conditions. It is not unusual to have an error of 5% or more, depending on the assumed profiles. Therefore, the situation is remedied by adjusting the multiplicative constant, namely, replacing 1 by 1.14. Thus, the following approximate formulae can be proposed:

$$\begin{cases} \dfrac{Nu_x}{Re_x^{\frac{1}{2}}} = \dfrac{1.14}{\delta_{\mathrm{T}}^*}, \\ \dfrac{Sh_x}{Re_x^{\frac{1}{2}}} = 1.14\dfrac{\Delta}{\delta_{\mathrm{T}}^*}. \end{cases} \tag{41}$$

As a comparison between the heat transfer coefficient of the base fluid and the heat transfer coefficient of the nanofluid, we introduce the enhancement ratio as follows:

$$\frac{h_{\mathrm{nf}}}{h_{\mathrm{f}}} = \frac{(\delta_{\mathrm{T}}^*)_{\mathrm{f}}}{(\delta_{\mathrm{T}}^*)_{\mathrm{nf}}}\frac{k_{\mathrm{nf}}}{k_{\mathrm{f}}}\sqrt{\frac{\upsilon_{\mathrm{f}}}{\upsilon_{\mathrm{nf}}}}, \tag{42}$$

where

$$h = \frac{k}{\delta_{\mathrm{T}}}, \quad \delta_{\mathrm{T}} = \delta_{\mathrm{T}}^*\frac{x}{\sqrt{Re_x}}, \quad \sqrt{Re_x} = \sqrt{\frac{a}{\upsilon}}x.$$

Combining the similarity approach with the boundary layer approximations used by Noghrehabadi et al.[18] and Khan and Pop[15] yields the enhancement ratio as follows:

$$\frac{h_{\mathrm{nf}}}{h_{\mathrm{f}}} = \frac{(\theta'(0))_{\mathrm{nf}}}{(\theta'(0))_{\mathrm{f}}}\frac{k_{\mathrm{nf}}}{k_{\mathrm{f}}}\sqrt{\frac{\upsilon_{\mathrm{f}}}{\upsilon_{\mathrm{nf}}}}, \tag{43}$$

where $\theta'(0)$ is the non-dimensional temperature gradient at the surface, and

$$\theta = \frac{T - T_\infty}{T_{\mathrm{w}} - T_\infty}.$$

3 Thermophysical properties

The thermophysical properties of the nanofluid are given in Table 1[23–24]. The density of the nanofluid is evaluated as follows[25]:

$$\rho_{\mathrm{nf}} = (1-\varphi)\rho_{\mathrm{f}} + \varphi\rho_{\mathrm{p}}. \tag{44}$$

The effective dynamic viscosity of nanofluids is evaluated by the Brinkman model[26–27] as follows:

$$\mu_{\mathrm{nf}} = \frac{\mu_{\mathrm{f}}}{(1-\varphi)^{2.5}}, \tag{45}$$

and the heat capacity of nanofluids $(\rho C_{\mathrm{p}})_{\mathrm{nf}}$ is computed by[28]

$$(\rho C_{\mathrm{p}})_{\mathrm{nf}} = (1-\varphi)(\rho C_{\mathrm{p}})_{\mathrm{f}} + \varphi(\rho C_{\mathrm{p}})_{\mathrm{p}}. \tag{46}$$

The nanofluid thermal conductivity is evaluated by the Maxwell model as follows[29–30]:

$$k_{\mathrm{nf}} = k_{\mathrm{f}}\frac{k_{\mathrm{p}} + 2k_{\mathrm{f}} - 2\varphi(k_{\mathrm{f}} - k_{\mathrm{p}})}{k_{\mathrm{p}} + 2k_{\mathrm{f}} + \varphi(k_{\mathrm{f}} - k_{\mathrm{p}})}, \tag{47}$$

where the subscripts f and p represent the base fluid and the nanoparticle, respectively, and the subscript nf denotes the nanofluid.

Table 1 Thermophysical properties of water and nanoparticles[23–24]

	$k/(\mathrm{W\cdot m^{-1}\cdot K^{-1}})$	$\rho/(\mathrm{kg\cdot m^{-3}})$	$C_\mathrm{p}/(\mathrm{J\cdot kg^{-1}\cdot K^{-1}})$	$\mu/(\mathrm{kg\cdot m^{-1}\cdot s^{-1}})$
Fluid phase (water)	0.613	997.1	4 179	1.002×10^{-3}
Al_2O_3	40	3 970	765	—
SiO_2	36	3 970	765	—
Ag	429	10 500	235	—
Cu	401	8 933	385	—

The Brownian and thermal diffusion coefficients are obtained from the following relations[25]:

$$D_\mathrm{B} = \frac{K_\mathrm{B} T_\infty}{3\pi\mu_\mathrm{nf} d_\mathrm{p}}, \tag{48}$$

$$D_\mathrm{T} = \beta\frac{\mu_\mathrm{nf}}{\rho_\mathrm{nf}}\varphi_\infty, \tag{49}$$

where K_B is the Boltzmann constant ($1.38\times10^{-23}\,\mathrm{J\cdot K^{-1}}$), d_p represents the nanoparticle diameter, and β is the thermophoretic coefficient evaluated as follows[25]:

$$\beta = 0.26\frac{k_\mathrm{f}}{2k_\mathrm{f}+k_\mathrm{p}}. \tag{50}$$

As a practical case, it is assumed that the temperature of the sheet T_w is 40 °C, and the ambient temperature T_∞ is 20 °C. The size of the nanoparticles is 30 nm, and the ambient volume fraction of the nanoparticles φ_∞ is the variable parameter. For convenience, the concentration difference $\Delta\varphi$ is assumed to be equal to the concentration of ambient, i.e., $\Delta\varphi = \varphi_\infty$. With Eqs. (44)–(50) and the thermo-physical properties listed in Table 1, the dimensionless parameters required in Eqs. (34) and (35) can be calculated (see Table 2).

Table 2 Nanofluid properties and non-dimensional parameters as function of type and volume fraction of nanoparticles

	φ	k_nf	v_nf	Pr	Le	N_T	N_B
	0.01	0.630 7	1.00×10^{-6}	6.592 7	71 859.93	1.97×10^{-6}	1.01×10^{-7}
Al_2O_3	0.03	0.667 2	9.95×10^{-7}	6.165 3	75 224.21	6.20×10^{-6}	2.90×10^{-7}
	0.05	0.705 2	9.94×10^{-7}	5.794 3	79 150.72	1.10×10^{-5}	4.60×10^{-7}
	0.01	0.630 6	1.00×10^{-6}	6.593 6	71 859.93	2.18×10^{-6}	1.01×10^{-7}
SiO_2	0.03	0.667 0	9.95×10^{-7}	6.167 9	75 224.21	6.93×10^{-6}	2.90×10^{-7}
	0.05	0.704 8	9.94×10^{-7}	5.798 3	79 150.72	1.12×10^{-5}	4.60×10^{-7}
	0.01	0.631 4	9.40×10^{-7}	6.182 6	67 563.31	1.54×10^{-7}	8.76×10^{-8}
Ag	0.03	0.669 6	8.43×10^{-7}	5.183 4	63 731.01	4.90×10^{-7}	2.78×10^{-7}
	0.05	0.709 3	7.73×10^{-7}	4.452 2	61 597.45	8.66×10^{-7}	4.80×10^{-7}
	0.01	0.631 5	9.54×10^{-7}	6.287 3	68 546.83	2.29×10^{-7}	1.20×10^{-7}
Cu	0.03	0.669 6	8.75×10^{-7}	5.418 9	66 156.57	7.31×10^{-7}	3.74×10^{-7}
	0.05	0.709 3	8.17×10^{-7}	4.758 6	65 059.81	1.29×10^{-6}	6.34×10^{-7}

The Prandtel number is a decreasing function of the nanoparticle volume fraction, while the Brownian motion parameter and the thermophoresis parameter are increasing functions of

the nanoparticle volume fraction. It is interesting that the trend of the variation of the Lewis number for different nanoparticles is different. The Lewis number is a decreasing function of the nanoparticle volume fraction in the case of Ag and Cu nanoparticles, while it is an increasing function of the nanoparticle volume fraction in the cases of Al_2O_3 and SiO_2. In fact, the Lewis number can be written as

$$\frac{3\pi d_{\mathrm{p}}}{K_{\mathrm{B}}T_{\infty}}\frac{\mu_{\mathrm{nf}}^2}{\rho_{\mathrm{nf}}}.$$

Therefore, for a specified size of nanoparticles (d_{p}) and a fixed reference temperature (T_{∞}), the Lewis number is solely a function of the dynamic viscosity and the density. It is clear that the augmentation of the nanoparticle volume fraction increases the dynamic viscosity. Moreover, in most cases, the density of the nanoparticles is much higher than the density of the base fluid. Therefore, the addition of heavy nanoparticles will intensify the density of the resulting nanofluid, and the increase in the volume fraction of nanoparticles will raise the dynamic viscosity and the density simultaneously. Therefore, the trend of the variation of the Lewis number for heavy nanoparticles with a very high density (metallic nanoparticles) is not the same as that for metallic oxide nanoparticles.

4 Results and discussion

The system of Eqs. (34) and (35) is solved with the practical dimensionless parameters listed in Table 2 to obtain Δ and δ_{T}^*. As a test of the accuracy of the solution, the values of Nu_{r} are compared with those data reported by Wang[13], Gorla and Sidawi[14], and Khan and Pop[15] in Table 3 when the effects of the thermophoresis parameter and the Brownian motion parameter are neglected. Table 3 shows that the present results are in good agreement with the results reported by the previous studies.

Table 3 Comparison of results for reduced Nusselt number (Nu_{r}) in pure fluid ($N_{\mathrm{B}} = N_{\mathrm{T}} = 0$)

Pr	Wang[13]	Gorla and Sidawi[14]	Khan and Pop[15]	Present study
0.2	0.169 1	0.169 1	0.169 1	0.169 495
0.7	0.453 9	0.453 9	0.453 9	0.449 663
2	0.911 4	0.911 4	0.911 3	0.901 709
7	1.895 4	1.895 6	1.895 4	1.886 892
20	3.353 9	3.353 9	3.353 9	3.356 245
70	6.462 2	6.462 2	6.462 1	6.493 741

Table 4 shows the calculated values of δ_{T}^* and δ_{C}^* for different type and volume fractions of nanoparticles dispersed in the water. The enhancement ratio is also calculated analytically. The results are given in Table 5. The similarity equations are boundary value, seventh-order, and highly non-linear. The similarity equations are solved by the Runge-Kutta-Fehlberg method and the shooting technique with an error less than 1.0×10^{-10}. The obtained accuracy of the numerical results is validated against the results reported by Khan and Pop[15] and Noghrehabadi et al.[18]. Based on the results of Table 5, we can find that the maximum value of the relative error is 1%. This error is not unusual, and it depends on the assumed profiles.

Figures 2 and 3 present the effects of the volume fraction of Al_2O_3 nanoparticles on the concentration distribution and the temperature distribution, respectively. The results show that the magnitude of the concentration profiles decreases smoothly when the volume fraction of the nanoparticles increases from 0.00 to 0.05.

Table 4 Thermal and concentration boundary layer coefficients for different types of nanoparticles

φ	Al_2O_3		SiO_2		Ag		Cu	
	$\frac{\delta_T^*}{\Delta} = \delta_C^*$	δ_T^*	$\frac{\delta_T^*}{\Delta}$	δ_T^*	$\frac{\delta_T^*}{\Delta}$	δ_T^*	$\frac{\delta_T^*}{\Delta}$	δ_T^*
0.01	0.005 736	0.624 9	0.005 786	0.624 8	0.005 487	0.648 0	0.005 452	0.641 9
0.03	0.005 623	0.649 0	0.005 676	0.648 9	0.005 648	0.716 6	0.005 548	0.698 6
0.05	0.005 504	0.672 4	0.005 556	0.672 1	0.005 593	0.782 3	0.005 743	0.752 7

Table 5 Enhancement ratio (h_{nf}/h_{bf}) for different types of nanoparticles

φ	Al_2O_3		SiO_2		Ag		Cu	
	Numeric	Analytic	Numeric	Analytic	Numeric	Analytic	Numeric	Analytic
0.01	1.011 1	1.011 0	1.011 0	1.010 9	1.007 1	1.006 6	1.009 3	1.008 9
0.03	1.032 7	1.032 3	1.032 6	1.032 1	1.020 9	1.019 3	1.027 7	1.026 3
0.05	1.054 6	1.053 6	1.543 9	1.053 5	1.035 3	1.032 9	1.046 2	1.044 2

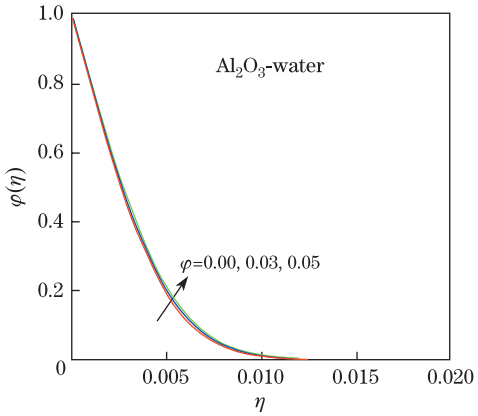

Fig. 2 Profiles of dimensionless concentration for selected values of volume fraction of Al_2O_3 nanoparticles

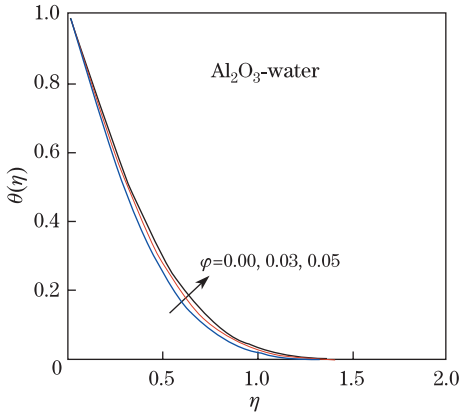

Fig. 3 Profiles of dimensionless temperature for selected values of volume fraction of Al_2O_3 nanoparticles

As the volume fraction of Al_2O_3 increases, the thermal conductivity increases, and consequently, the thermal boundary layer thickness increases. An increase in the volume fraction of Al_2O_3 nanoparticles will decrease the thickness of the concentration boundary layer. These results are in good agreement with the results listed in Table 4. The same trend of results is observed for SiO_2 nanoparticles. Therefore, the concentration and temperature profiles for SiO_2 are omitted here.

The effects of the volume fraction of Ag nanoparticles on the concentration and temperature distributions are illustrated in Figs. 4 and 5, respectively. These figures reveal that an increase in the volume fraction of the nanoparticles will increase the thickness of the thermal and concentration boundary layers. The same trend of results is observed in the case of Cu nanoparticles. In the case of Ag nanoparticles, the variation trend of the concentration boundary layer thickness is not in agreement with that of Al_2O_3 nanoparticles. This is because that the Lewis number is an increasing function of the nanoparticle volume fraction in the case of metallic oxide nanoparticles (Al_2O_3 and SiO_2) while a decreasing function of the nanoparticle volume fraction in the case of metallic nanoparticles (Ag and Cu) (see Table 2).

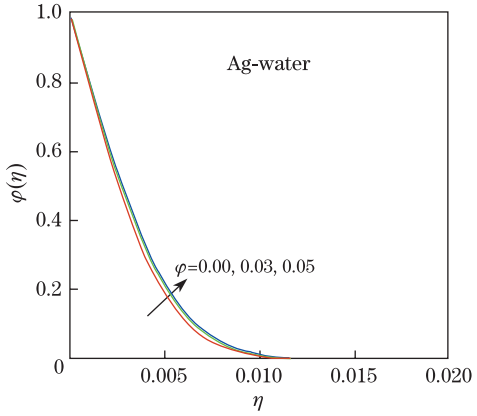

Fig. 4 Profiles of dimensionless concentration for selected values of volume fraction of Ag nanoparticles

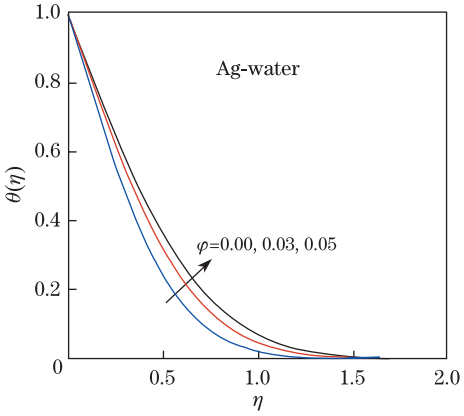

Fig. 5 Profiles of dimensionless temperature for selected values of volume fraction of Ag nanoparticles

Figures 6 and 7 display the behaviors of the concentration profiles and the temperature profiles with different nanofluids for $\varphi = 0.05$. These figures show that different types of nanoparticles have different significant effects on the variations of the concentration and temperature profiles. The thickness of the boundary layer for the concentration of nanoparticles is found to be smaller than that of the thermal boundary layer thickness when $Le > 1$.

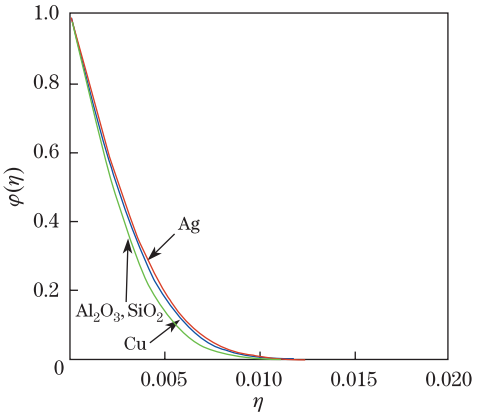

Fig. 6 Concentration $\varphi(\eta)$ profiles for different types of nanoparticles when $\varphi_\infty = 0.05$

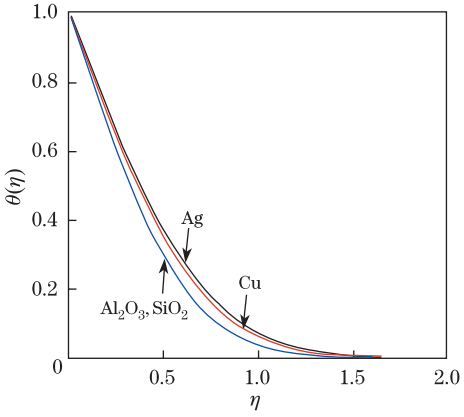

Fig. 7 Temperature $\theta(\eta)$ profiles for different types of nanoparticles when $\varphi_\infty = 0.05$

The reduced Nusselt number as a function of the volume fraction of nanoparticles is depicted in Fig. 8. This figure reveals that an increment in the volume fraction of nanoparticles will decrease the magnitude of the reduced Nusselt number for all investigated types of nanoparticles when the nanoparticle volume fraction increases. Then, when the thermal boundary layer thickness increases, the reduced Nusselt number decreases. As seen in the figure, these results are in good agreement with the variation of the thickness of the thermal boundary layer. It is clear that the decrease in the reduced Nusselt number for Ag nanoparticles is very significant.

The effects of the nanoparticle volume fraction on the reduced Sherwood number for different types of nanoparticles are illustrated in Fig. 9. This figure interestingly shows that the increase

in the nanoparticle volume fraction decreases the reduced Sherwood number in the cases of Cu-water and Ag-water nanofluids, while the reduced Sherwood number is an increasing function of the volume fraction of nanoparticles in the cases of Al_2O_3-water and SiO_2-water nanofluids. This is because that the increase in the nanoparticle volume fraction will decrease the thickness of the concentration boundary layer in the cases of Al_2O_3-water and SiO_2-water nanofluids; however, it increases the thickness of the concentration boundary layer in the cases of Cu-water and Ag-water nanofluids.

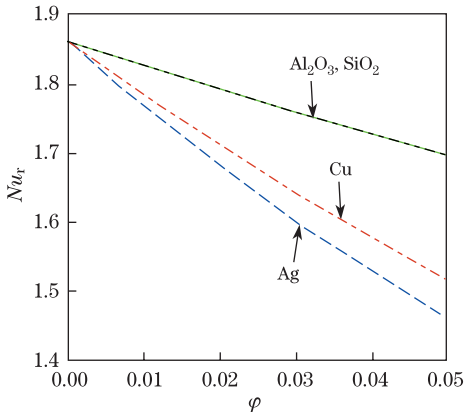

Fig. 8 Reduced Nusselt number profiles for various values of φ

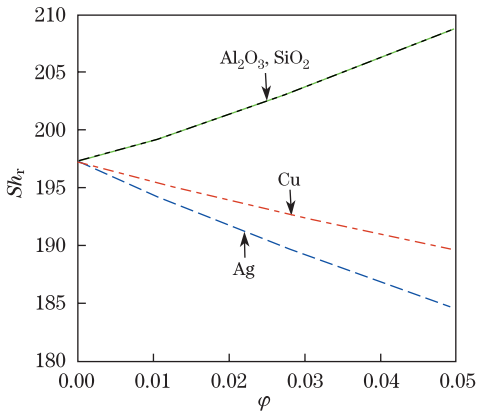

Fig. 9 Reduced Sherwood number profiles for various values of φ

5 Conclusions

The effects of metallic oxide (Al_2O_3 and SiO_2) and metallic (Ag and Cu) nanoparticles on the concentration and thermal boundary layer over an isothermal stretching sheet are analytically investigated. The advantage of the present integral method is that it successfully provides an analytic approximate solution to the highly non-linear governing equations. The analytical solution is non-dimensional. Therefore, the obtained results can be easily utilized for different nanofluids and temperature boundary conditions in practical applications. The results indicate that there is a significant difference between the metallic and metallic oxide nanoparticles on the trend of the concentration thickness of the boundary layer. An increase in the nanoparticle volume fraction will raise the concentration boundary layer thickness in the case of metallic nanoparticles. In contrast, an augmentation of the volume fraction of nanoparticles will reduce the thickness of the concentration boundary layer in the case of metallic oxide nanoparticles. For all investigated types of nanoparticles, an increase in the nanoparticle volume fraction will raise the thickness of the thermal boundary layer. The effects of variations of the nanoparticle volume fraction are also examined on the heat and mass transfer rate for different types of nanoparticles. It is found that metallic oxide nanoparticles (Al_2O_3 and SiO_2) prove higher cooling performance than metallic (Ag and Cu) nanoparticles over a stretching sheet.

References

[1] Altan, T., Oh, S. I., and Gegel, H. L. *Metal Forming: Fundamentals and Applications*, ASM International, Ohio (1979)

[2] Fisher, E. G. *Extrusion of Plastics*, Wiley, New York (1976)

[3] Karwe, M. V. and Jaluria, Y. Numerical simulation of thermal transport associated with a continuous moving flat sheet in materials processing. *Journal of Heat Transfer*, **119**, 612–619 (1991)

[4] Choi, S. U. S. Enhancing thermal conductivity of fluids with nanoparticle. *Developments and Applications of Non-Newtonian Flows*, **231**, 99–105 (1995)

[5] Eastman, J. A., Choi, S. U. S., Li, S., Yu, W., and Thompson, L. J. Anomalously increased effective thermal conductivities containing copper nanoparticles. *Applied Physics Letters*, **78**, 718–720 (2001)

[6] Choi, S. U. S., Zhang, Z. G., Yu, W., Lockwood, F. E., and Grulke, E. A. Anomalous thermal conductivity enhancement on nanotube suspension. *Applied Physics Letters*, **79**, 2252–2254 (2001)

[7] Sun, C. Z., Bai, B. F., Lu, W. Q., and Liu, J. Shear-rate dependent effective thermal conductivity of H_2O+SiO_2 nanofluid. *Physics of Fluids*, **25**, 052002 (2013)

[8] Sakiadis, B. C. Boundary-layer behavior on a continuous solid surface: II, the boundary layer on a continuous flat surface. *AIChE Journal*, **7**, 221–225 (1961)

[9] Crane, L. J. Flow past a stretching plate. *Zeitschrift für Angewandte Mathematik und Physik*, **21**, 645–647 (1970)

[10] Tsou, F. K., Sparrow, E. M., and Goldstein, R. J. Flow and heat transfer in the boundary layer in the continuous moving surfaces. *International Journal of Heat and Mass Transfer*, **10**, 219–235 (1967)

[11] Magyari, E. and Keller, B. Heat and mass transfer in the boundary layers on an exponentially stretching continuous surface. *Journal of Physics D*: *Applied Physics*, **32**, 577–585 (1999)

[12] Magyari, E. and Keller, B. Heat transfer characteristics of the separation boundary flow induced by a continuous stretching surface. *Journal of Physics D*: *Applied Physics*, **32**, 2876–2881 (1999)

[13] Wang, C. Y. Free convection on a vertical stretching surface. *Journal of Applied Mathematics and Mechanics*, **69**, 418–420 (1989)

[14] Gorla, R. S. R. and Sidawi, I. Free convection on a vertical stretching surface with suction and blowing. *Applied Scientific Research*, **52**, 247–257 (1994)

[15] Khan, W. A. and Pop, I. Boundary-layer flow of a nanofluid past a stretching sheet. *International Journal of Heat and Mass Transfer*, **53**, 2477–2483 (2010)

[16] Makinde, O. D. and Aziz, A. Boundary-layer flow of a nanofluids past a stretching sheet. *International Journal of Thermal Sciences*, **50**, 1326–1332 (2011)

[17] Rana, P. and Bhargava, R. Flow and heat transfer of a nanofluids over nonlinearly stretching sheet: a numerical study. *Communications in Nonlinear Science and Numerical Simulation*, **17**, 212–226 (2012)

[18] Noghrehabadi, A. R., Pourrajab, R., and Ghalambaz, M. Effect of partial slip boundary condition on the flow and heat transfer of nanofluids past stretching sheet prescribed constant wall temperature. *International Journal of Thermal Sciences*, **54**, 253–261 (2012)

[19] Noghrehabadi, A. R., Ghalambaz, M., and Ghanbarzadeh, A. Heat transfer of magnetohydrodynamic viscous nanofluids over an isothermal stretching sheet. *Journal of Thermophysics and Heat Transfer*, **26**, 686–689 (2012)

[20] Noghrehabadi, A. R., Saffarian, M. R., Pourrajab, R., and Ghalambaz, M. Entropy analysis for nanofluid flow over a stretching sheet in the presence of heat generation/absorption and partial slip. *Journal of Mechanical Science and Technology*, **27**, 927–937 (2013)

[21] Noghrehabadi, A. R., Pourrajab, R., and Ghalambaz, M. Flow and heat transfer of nanofluids over stretching sheet taking into account partial slip and thermal convective boundary conditions. *Heat and Mass Transfer*, **49**, 1357–1366 (2013)

[22] Bejan, A. *Convection Heat Transfer*, Wiley, New York (2004)

[23] Oztop, H. F. and Abu-Nada, E. Numerical study of natural convection in partially heated rectangular enclosures filled with nanofluids. *International Journal of Heat and Fluid Flow*, **29**, 1326–1336 (2008)

[24] Kefayati, G. H., Hosseinzadeh, S. F., Gorji-Bandpy, M., and Sajjadi, H. Lattice Boltzman solution of natural convection in tall enclosures using water/SiO_2 nanofluid. *International Communications in Heat and Mass Transfer*, **38**, 798–805 (2011)

[25] Buongiorno, J. Convective transport in nanofluids. *Journal of Heat Transfer*, **128**, 240–250 (2006)

[26] Brinkman, H. C. The viscosity of concentrated suspensions and solutions. *Journal of Chemical Physics*, **20**, 571–581 (1952)

[27] Khanafer, K. and Vafai, K. A critical synthesis of thermophysical characteristics of nanofluids. *International Journal of Heat and Mass Transfer*, **54**, 4410–4428 (2011)

[28] Yacob, N. A., Ishak, A., Pop, I., and Vajravelu, K. Boundary layer flow past a stretching/shrinking surface beneath an external uniform shear flow with a convective surface boundary condition in a nanofluids. *Nanoscale Research Letters*, **6**, 314–321 (2011)

[29] Maxwell, J. C. A. *Treatise on Electricity and Magnetism*, 2nd ed., Clarendon Press, Oxford (1881)

[30] Buongiorno, J., Venerus, D. C., Prabhat, N., McKrell, T., Townsend, J., Christianson, R., and Leong, K. C. A benchmark study on the thermal conductivity of nanofluids. *Journal of Applied Physics*, **106**, 094312 (2009)